AD-A261 812

NTATION PAGE

Form Approved
OMB No. 0704-0188

ORT DATE	3. REPORT TYPE AND DATES COVERED
Nov. 16, 1992	Final Technical Report July 1, 1991-June 30, 1992

4. TITLE AND SUBTITLE
Bayesian Cross-Entropy Reconstruction of Complex Images

5. FUNDING NUMBERS
N00014-91-J-4056

6. AUTHOR(S)
B. Roy Frieden

7. PERFORMING ORGANIZATION NAME(S) AND ADDRESS(ES)
The University of Arizona
Optical Sciences Center
Tucson, Arizona 85721

8. PERFORMING ORGANIZATION REPORT NUMBER

9. SPONSORING/MONITORING AGENCY NAME(S) AND ADDRESS(ES)
Department of the Navy
Office of Naval Research
Resident Representative
University of New Mexico, Bandelier Hall West
Albuquerque, NM 87131

10. SPONSORING/MONITORING AGENCY REPORT NUMBER

11. SUPPLEMENTARY NOTES
Copy of report provided to scientific officer, Bill Miceli, Nov. 16, 1992
Two copies of report provided to Defense Technical Information Center, March 4, 1993

12a. DISTRIBUTION/AVAILABILITY STATEMENT
approved for public release; distribution unlimited

12b. DISTRIBUTION CODE

13. ABSTRACT *(Maximum 200 words)*

Bajkova's generalized maximum entropy method (GMEM) for reconstruction of complex signals has been further generalized through the use of Kullback-Leibler cross entropy. This permits a priori information in the form of bias functions to be inserted into the algorithm, with resulting benefits to reconstruction quality. Also, the cross-entropy term is imbedded within an overall m.a.p. (maximum a posteriori probability) approach that includes a noise-rejection term. A further modification is transformation of the large, two-dimensional problem due to modest-sized 2-D images into a sequence of one-dimensional problems. Finally, the added operation of three-point median window filtration of each intermediary, one-dimensional output is shown to suppress edge-top overshoots while augmenting edge gradients. Applications to simulated complex images are shown.

14. SUBJECT TERMS			15. NUMBER OF PAGES 32
			16. PRICE CODE
17. SECURITY CLASSIFICATION OF REPORT unclassified	18. SECURITY CLASSIFICATION unclassified	19. SECURITY CLASSIFICATION OF ABSTRACT unclassified	20. LIMITATION OF ABSTRACT n/a

Bayesian Cross-Entropy Reconstruction of Complex Images

B. Roy Frieden

Optical Sciences Center, The University of Arizona

Tucson, Arizona 85721

Anisa T. Bajkova

Institute of Applied Astronomy of the USSR Academy of Sciences

St. Petersburg 197042, Russia

Abstract

Bajkova's generalized maximum entropy method (GMEM) for reconstruction of complex signals has been further generalized through the use of Kullback-Leibler cross entropy. This permits a priori information in the form of bias functions to be inserted into the algorithm, with resulting benefits to reconstruction quality. Also, the cross-entropy term is imbedded within an overall m.a.p. (maximum a posteriori probability) approach that includes a noise-rejection term. A further modification is transformation of the large, two-dimensional problem due to modest-sized 2-D images into a sequence of one-dimensional problems. Finally, the added operation of three-point median window filtration of each intermediary, one-dimensional output is shown to suppress edge-top overshoots while augmenting edge gradients. Applications to simulated complex images are shown.

Introduction

Complex signals occur widely in electromagnetic phenomena. It is often required to estimate such signals from incomplete data in a conjugate space. As examples: In interactive synthetic aperture radar (ISAR)[1] the complex Fourier transform of a spatial amplitude image is known within a band of frequencies, and from this data the complex image is to be estimated. In radio astronomy, the data are complex amplitudes in an unfilled Fourier space as dictated by the earth's motion[2]. In Fourier transform holography, the hologram might have missing or damaged regions. In quantum mechanics, the spatial wave function of a particle is to be estimated from incomplete knowledge of momentum (Fourier) space for the particle. In these examples, the conjugate space to the required signal is Fourier space. Although the processing approach described below applies to any linear conjugate space, because of its central importance we will continue the development specifically for the Fourier-space problem. Because of the incomplete knowledge of Fourier space we seek a processing approach that allows for bandwidth interpolation and extrapolation.

Entropic Processing

Since its first use in image restoration[3], maximum entropy has been known to be capable of extrapolation in Fourier space. It also produces maximally smooth, or unbiased, estimates[3,4]. If f(t) is a real signal to be estimated, then the maximum entropy solution $\hat{f}(t)$ is to satisfy

$$-\int dt\, f(t) \ln f(t) = H = Max., \quad f(t) \geq 0, \tag{1}$$

subject to constraints on f(t) provided by the Fourier data. (All integrals have infinite limits

unless otherwise specified.) Quantity H is the (real) Shannon entropy of the signal. As noted, the signal must be real and positive-definite for a real H to exist. Methods of achieving maximum entropy estimation in different senses than (1) also exist. Among these are Burg's[5] *ln x(t)*-form of entropy and Borden's[6] probabilistic model approach. In this paper, we stick with form (1) of entropy because of its widespread use in signal estimation problems[7].

The formulation (1) of maximum entropy has, in the past, been exclusively applied to positive-definite, real signals such as probability densities[8], power spectra[5], and intensity images[3,9]. However, here we want to work with the Shannon entropy of a *complex* signal. How can this be done?

Recently, Bajkova[10] showed how to accomplish this objective. We describe her approach first, and then formulate an improved version for application to noisy, two-dimensional complex images.

GMEM Processing

First, consider a *real* signal r(t), as in Fig. 1, that is to be estimated. It is generally bipolar, with positive and negative values as indicated. Such a signal can be represented as the difference between two positive-definite functions

$$r(t) = x(t) - y(t), \quad x(t) \geq 0, \; y(t) \geq 0. \tag{2}$$

Thus, the positive regions in Fig. 1 are represented by r(t), the negative by y(t). Curves x(t) and y(t) do not, of course, have overlapping support regions. *Let us replace the problem of estimating r(t) by one of estimating x(t) and y(t).* Then for any estimates of x(t), y(t) to be valid, they must have *non*-overlapping support regions and must be positive-definite.

The latter constraint allows the entropy

$$-\int dt\, x(t)\, ln\, x(t) - \int dt\, y(t)\, ln\, y(t) \tag{3a}$$

to exist. Hence, maximum entropy processing can be applied to these signals, aiding our overall objective. Furthermore, since x(t) and y(t) do not overlap, the entropy integral (3a) is the entropy of the absolute value of r(t) as well,

$$-\int dt\, |\, r(t)\, |\, ln\, |\, r(t)\, |\, = H(r). \tag{3b}$$

Thus, maximizing the entropy H(r) is equivalent to maximizing the sum of the entropies of x(t) and y(t). This would allow each constituent x(t), y(t) of the required signal r(t) to be separately estimated by maximum entropy. Again, this is despite the fact that r(t) may have negative regions. Hence, we adapt the maximization of (3b) as our criterion.

The extension to the full-blown complex problem is straightforward. Consider a complex signal

$$u(t) = r(t) + jq(t), \quad j = \sqrt{-1}, \tag{4}$$

r(t), q(t) real and generally bipolar. We wish to estimate u(t). Equivalently, we may choose to estimate r(t) and q(t). Represent r(t) as in Eq. (2), and similarly represent

$$q(t) = z(t) - v(t), \quad z(t) \geq 0, \quad v(t) \geq 0. \tag{5}$$

The entropy of the absolute value of r(t) still obeys both Eqs. (3a,b). Likewise the entropy of the absolute value of q

$$H(q) = -\int dt \mid q(t) \mid ln \mid q(t) \mid \tag{6}$$

also obeys

$$H(q) = -\int dt\, z(t)\, ln\, z(t) - \int dt\, v(t)\, ln\, v(t), \tag{7}$$

providing z(t), v(t) do not overlap. Hence, maximizing the entropy H(q) accomplishes an entropic estimate of q(t).

Since our objective is to estimate the complex u(t), we have to estimate both real and imaginary parts r(t) and q(t). This suggests that we adopt one grand principle of maximizing the sumtotal entropy H(r) plus H(q), or

$$\begin{aligned} H(u) &= H(r) + H(q) \\ &= -\int dt [x(t)\, ln\, x(t) + y(t)\, ln\, y(t) + z(t)\, ln\, z(t) + v(t)\, ln\, v(t)] \\ &= Max. \end{aligned} \tag{8}$$

Next, recall the nonoverlapping support requirements for x(t), y(t) and for z(t), v(t). This would not necessarily be met by simply maximizing the form (8). It was empirically found[7] that a 'tuning parameter' α must be inserted, to form an associated entropy

$$\begin{aligned} H(u;\alpha) &= -\int dt\, \{x(t)\, ln\, [\alpha x(t)] + y(t)\, ln[\alpha y(t)] + z(t)\, ln\, [\alpha z(t)] + v(t)\, ln\, [\alpha v(t)]\}. \\ &= Max. \end{aligned} \tag{9}$$

The value of α is at the discretion of the user. Empirically, the action of α is to force nonoverlap as α is made larger. Also, a large α causes better data agreement and, hence, higher resolution in the output u(t). This is because the principle (9) will be constrained by

higher resolution in the output u(t). This is because the principle (9) will be constrained by input data as well, and the data are more closely obeyed when mathematical constructions (2) and (5) for r(t) and q(t) are valid (i.e., when the functions do not overlap). This was empirically borne out by computer simulations described below.

GMEMK Processing

Generally speaking, the insertion into an algorithm of *a priori* truth about an unknown signal can only improve the algorithm. Thus, Kullback-Leibler information[11] allows for the insertion of a prior bias function g(t) into the ordinary entropy form, as

$$H_{KL}(f) = -\int dt\, f(t)\, ln\, [f(t)/g(t)], \quad f(t) \geq 0,\ g(t) \geq 0. \tag{10}$$

[Compare with Eq. (1).] As will be seen, maximizing H_{KL} subject to linear data constraints produces a solution f(t) that is linearly proportional to input function g(t). Hence, g(t) acts to 'bias' f(t) toward its peaks and valleys. Thus, for it to exert a proper influence upon f(t), bias g(t) should be a first approximation to f(t), say, by a linear method.

In our problem, we likewise assume prior knowledge of bias functions a(t), b(t), c(t), d(t), corresponding to signals x(t), y(t), z(t), v(t) respectively. Then the principle (9) is modified as

$$H_{KL}(u;a) = -\int dt\, \{x(t)\, ln\, [ax(t)/a(t)] + y(t)\, ln\, [ay(t)/b(t)] + z(t)\, ln\, [az(t)/c(t)] + v(t)\, ln\, [av(t)/d(t)]\} = Max. \tag{11}$$

It is particularly easy to form appropriate bias functions for our problem. These are simply the smoothed, inverse-Fourier transforms of the Fourier data. Missing data regions are simply padded in with zeros (see below).

Eq. (11) is, thus, a generalized maximum entropy method in the spirit of Kullback, and hence is named GMEMK (see also Refs. 12-15). We next consider how data inputs are built into the algorithm.

Data Constraints

Principle (11) by itself is incomplete. We want the solution x(t), y(t), z(t), v(t) that satisfies (11) *subject to observable data* as well. There appear to be two schools of thought on how to implement data constraints. One way is to lump them into one merit function, usually called chi-square[9], which is the mean-square discrepancy between the observed data and the data as implied by a given solution. This term is subtracted from (11) and the result is maximized. A second approach is to add each data constraint to (11) via a Lagrange multiplier term, and to then maximize the sum[3]. We take the latter approach.

As mentioned at the outset, we specialize the approach to the case of Fourier-space data, at frequencies ω_m, m = 1,...,M. Denote the data as D^r_m, D^i_m, m = 1,...,M, where superscripts r and i denote real and imaginary parts, respectively. Allow for the presence of additive noise η^r_m, η^i_m as well. Then the data equations are

$$\begin{aligned} D^r_m &= \int dt\,[x(t) - y(t)]\,\cos\omega_m t - \int dt\,[z(t) - v(t)]\,\sin\omega_m t + \eta^r_m \\ D^i_m &= \int dt\,[x(t) - y(t)]\,\sin\omega_m t + \int dt\,[z(t) - v(t)]\,\cos\omega_m t + \eta^i_m \\ m &= 1,\ldots,M \end{aligned} \tag{12}$$

These must be satisfied by any solution x(t), y(t), z(t), r(t). The data constraints (12) will be appended to the net estimation principle in the conventional way, as additive Lagrange multiplier terms.

Noise Rejection; M.a.p. Estimation

It is important to build a noise rejection mechanism into any restoring algorithm. This acts to further regularize the outputs over and above what maximizing entropy can do. Again, there appear to be two schools of thought on how to accomplish this.

In general, noise rejection is enforced by permitting the computed data, as inferred by a particular solution, to depart from the observed data. This 'slippage' in data consistency reduces the resolution of the output, but with the benefit of smoothing out noise contributions. If a chi-square merit function is used, this by itself allows for noise rejection since chi-square (measure of data inconsistency) is allowed to be finite at solution.

By comparison, the Lagrange approach (below) permits slippage because the noise components η^r_n, η^r_n are separately estimated, and allowed to be finite. The Lagrange approach is also used in conjunction with an added log-likelihood noise term to the objective merit function (11), to further regularize the problem[16]. Assume the presence of additive, circular Gaussian noise. Let σ_m^2 be the noise variances for each of the real and imaginary parts at frequencies ω_m. Then the net estimation principle becomes

$$H_{KL}(u;a) - \frac{1}{2}\sum_{m=1}^{M}\left(\eta_m^{r\,2} + \eta_m^{i\,2}\right)/\sigma_m^2 = Max. \qquad (13)$$

This is equivalent to seeking a solution u,η^r,η^i that maximizes the joint probability of unknown signals x(t), y(t), z(t), v(t) *and* noise values η^r_m, η^i_m[16]. By Bayes' theorem[7] with a prior probability law for u given by exp $[H_{KL}(u;a)]$, this is also a m.a.p. (maximum *a posteriori* probability) estimate of the unknowns. This approach mirrors that of Trussell[17] for incorporating ordinary MEM into a m.a.p. algorithm.

Net GMEMK Algorithm

In practice, the unknown signal is to be estimated at a finite-spaced subdivision of points $t = t_n = n\Delta t$, $n = 1,\ldots,N$. The frequencies $\omega = \omega_m = m\Delta\omega$, $\Delta\omega$ the frequency spacing, $m = 1,\ldots,M$, are also discrete. In addition, we consider undetermined problems, where the number of data values is less than or equal to the number of unknown signal values,

$$M \leq N. \tag{14}$$

Then, in the usual way, all integrals over t are replaced by sums over n. The estimation principle (13), as augmented by Lagrange data constraints (12), becomes

$$\begin{aligned}
&-\sum_{n=1}^{N}\left[x_n \ln(ax_n/a_n) + y_n \ln(ay_n/b_n) + z_n \ln(az_n/c_n) + v_n \ln(av_n/d_n)\right] \\
&+\sum_{m=1}^{M}\lambda_m\left[\sum_{n=1}^{N}\left[(x_n - y_n)\cos\omega_m t_n - (z_n - v_n)\sin\omega_m t_n\right] + \eta_m^r - D_m^r\right] \\
&+\sum_{m=1}^{M}\mu_m\left[\sum_{n=1}^{N}\left[(x_n - y_n)\sin\omega_m t_n + (z_n - v_n)\cos\omega_m t_n\right] + \eta_m^i - D_m^i\right] \\
&-\frac{1}{2}\sum_{m=1}^{M}\left(\eta_m^{r\,2} + \eta_m^{i\,2}\right)/\sigma_m^2 = G = Max.
\end{aligned} \tag{15}$$

This is the working estimation principle of the paper. Parameters λ_m and μ_m are conventional Lagrange multipliers. They will be seen to define our estimated signal, and to be determined by satisfaction of data equations (12).

Solution

Principle (15) is to be maximized through choice of all the unknowns: signals x_n, y_n, z_n, v_n, noise quantities η^r_m and η^i_m, and multipliers λ_m, μ_m. Accordingly, we set

$$\frac{\partial G}{\partial x_n} = \frac{\partial G}{\partial y_n} = \frac{\partial G}{\partial z_n} = \frac{\partial G}{\partial v_n} = 0, \qquad n = 1,\ldots,N. \tag{16}$$

These directly give a solution

$$\begin{aligned}
\hat{x}_n &= a_n \exp\left[-1 - \ln a + \sum_m \left(\lambda_m \cos\omega_m t_n + \mu_m \sin\omega_m t_n\right)\right] \\
\hat{y}_n &= a_n b_n \left(e^2 a^2 \hat{x}_n\right)^{-1} \\
\hat{z}_n &= c_n \exp\left[-1 - \ln a - \sum_m \left(\lambda_m \sin\omega_m t_n - \mu_m \cos\omega_m t_n\right)\right] \\
\hat{v}_n &= c_n d_n \left(e^2 a^2 \hat{z}_n\right)^{-1}.
\end{aligned} \tag{17}$$

Hence, the signal is defined by the Lagrange multipliers.

Setting

$$\frac{\partial G}{\partial \eta^r_m} = \frac{\partial G}{\partial \eta^i_m} = 0 \tag{18}$$

gives estimated noise values

$$\hat{\eta}^r_m = \sigma^2_m \lambda_m, \quad \hat{\eta}^i_m = \sigma^2_m \mu_m. \tag{19}$$

Thus, both signal (17) and noise (19) are defined by the Lagrange multipliers.

Finally, setting

$$\frac{\partial G}{\partial \lambda_m} = \frac{\partial G}{\partial \mu_m} = 0 \tag{20}$$

gives the condition that data Eqs. (12) (integrals replaced by sums) must be satisfied.

The upshot is that the estimation problem has been parametrized. All signal and noise unknowns are expressed, via Eqs. (17) and (19), in terms of the unknown multipliers λ_m and μ_m. These, in turn, are found by substituting the parameterized equations (17) and (19) into the data equations (12). The result is an algebraic set of 2M data equations (M each for real and imaginary parts) in 2M unknowns λ_m, μ_m. With an equal number of equations and unknowns, a unique solution is formally possible. We found this to be empirically true, as well. A Newton-Raphson[18] algorithm was written for solution of the equations. It was found to always converge to the same solution, regardless of starting solution.

Equations (17) show that for any (real) solution $\{\lambda_m\}$, $\{\mu_m\}$ to the problem, necessarily

$$\hat{x}_n \geq 0, \quad \hat{y}_n \geq 0, \quad \hat{z}_n \geq 0, \quad \hat{v}_n \geq 0. \tag{21}$$

All the reconstructed signals are positive-definite. This is important because positive-constrained solutions, being nonlinear in the data, can have higher bandwidth (and, hence, higher resolution) than the data. Maximum-entropy reconstruction often exhibit such resolution (3, 9, 12). By Eqs. (2) and (5), this will now be true for amplitudes r(t) and q(t), and hence for *complex signal* u(t), as well. Recall that this was one of our aims (see Introduction).

Two-dimensional implementation as sequence of 1-D problems

The notation has, so far, been one-dimensional. In principle, two dimensional data D^r_{mn}, D^i_{mn}, can be processed by the straightforward double-subscripting of all single-subscripted quantities above. However, the result would be a requirement to solve (now) $2M^2$ data equations in $2M^2$ unknowns, a formidable problem for even modest-sized pictures of $M \sim 64$ pixels on a side.

A way to surmount this problem of implementation is to break up the one, two-dimensional problem into a sequence of one-dimensional problems. Note that the Fourier data problem under consideration has a separable imaging kernel

$$\exp\,[j(\omega_1 t_1 + \omega_2 t_2)] = \exp\,(j\omega_1 t_1) \cdot \exp\,(j\omega_2 t_2), \tag{22}$$

where t_1 denotes (now) row coordinate and t_2 denotes column coordinate. The 2-D problem

$$\int\int dt_1\, dt_2\, u(t_1,t_2)\, e^{j(\omega_1 t_1 + \omega_2 t_2)} = D(\omega_1,\omega_2) \tag{23}$$

of estimating $u(t_1, t_2)$ may then be re-cast as

$$\int dt_1 e^{j\omega_1 t_1}\, E(t_1;\omega_2) = D(\omega_1;\omega_2), \tag{24a}$$

where

$$\int dt_2\, e^{j\omega_2 t_2}\, u(t_1,t_2) = E(t_1;\omega_2). \tag{24b}$$

This implies the following procedure for obtaining a solution $u(t_1, t_2)$.

First solve Eq. (24a) for the complex quantity $E(t_1; \omega_2)$ at each (row) $\omega_2 = m\Delta\omega$, m = 1,...,M. This is a sequence of M 1-D problems of size 2M. The solutions $E(t_1; \omega_2)$ are stored in an intermediary matrix. These are then used to form the right-hand sides of Eq. (24b), which is then solved for $u(t_1, t_2)$ at each (column) $t_2 = n\Delta t$, n = 1,...,N. This is a sequence of N 1-D problems of size 2M. The net effect is that the original 2-D problem of $2M^2$ unknowns in $2M^2$ equations is replaced by (M+N) one-dimensional problems of size 2M each. This procedure was followed below.

Demonstrations

Fourier images were formed, and processed, on a Convex C240 mini-super computer. The object was always the 64x64 pixel airplane silhouette shown in Fig. 2. This is a complex signal of real-part +1 and imaginary part -1 within the airplane outline, and 0 outside. All images show the modulus signal. This is usually the output of interest, e.g., in ISAR (inverse synthetic aperture radar) images. Note also the point source to the right of the airplane nose in Fig. 2. Edges and point sources are strong carriers of pattern shape information, and hence are crucial for purposes of pattern recognition. Overall, then, this image is contrived to test the GMEMK algorithm on a combined edge-point source object input.

The general objective was to form Fourier data from the complex object in Fig. 2, both without and with noise, and to observe the ability of the GMEMK algorithm to reconstruct the object under these conditions. Also, to more critically test the algorithm, we blanked out half the frequency-space of data values, and so attempted to reconstruct on a twice-as-fine basis as the data would ordinarily permit. Hence, we attempted bandwidth extrapolation, by a factor of two, in both resolution directions.

As will be discussed, the GMEMK algorithm can be augmented by a median window filter step, after each row or column reconstruction, so as to suppress Gibbs artifact oscillations that are induced by GMEMK (or any other reconstruction algorithm) at the edge tops.

Noise free data

The first demonstration is a noise-free one. The 64x64 pixel complex object of Fig. 2 is Fourier transformed, to give the spectrum shown in Fig. 3. The *logarithm* of the modulus is displayed for better viewing.

The black picture frame indicates blanked out data. Only the central 32x32 spectral values shown are used as data inputs to GMEMK. However, the reconstruction will still be on the 64x64 pixel basis. The aim is to regain the resolution apparently lost by blanking out the picture frame data values.

The conventional, linear output for the problem is first shown. This is the inverse, discrete Fourier transform (DFT) of the data. For example, in ISAR imaging, after the data are estimated in Fourier space, a DFT is ordinarily performed to produce the output image in direct space[1]. The picture frame region of unknown data was accommodated by simply assuming that all values are zero there. This 'zero padding' method is the usual one for artificially increasing output picture size using the DFT. The DFT of the data in Fig. 3 is shown in Fig. 4.

In this noise-free case, noise throughput in Fig. 4 is not a problem, but there is a notable loss of resolution at the airplane edges, and of the isolated point source. Of course this is due to loss of the outer frequencies (picture frame) in data space. Note also the artifact oscillations immediately around the airplane. These are also caused by the missing frequencies.

The GMEMK output for the problem is shown (in modulus) in Fig. 5. This used the complex output of Fig. 4 as bias functions $a_n,\ldots, d_n$ in the algorithm (15). Actually, the use of unity everywhere for the bias functions worked just as well in this noise-free case. The edges are now significantly improved in resolution, as is the isolated point source. The data bandwidth of size 32x32 in Fig. 3 has been effectively increased, although not to the full 64x64 size. This bandwidth augmentation follows from the *non*-bandlimited representation (17) for the bipolar functions $x_n,\ldots, v_n$ that form the complex output. (That is, e-to a general Fourier series is not bandlimited.) Note also the lack of artifact oscillations in the region surrounding the airplane (compare with Fig. 4).

The main drawback to the reconstruction in Fig. 5 is the presence of overshoot artifacts at the edge tops just within the airplane. Most (but not all[19]) reconstruction algorithms suffer from such edge artifacts. However, we were able to remove these by the use of an additional operation to GMEMK. This is to filter each complex GMEMK (row or column) output with a three-point median window[20]. This is a non-linear operation. Both real and imaginary parts are separately filtered. A median window filter is well-known to suppress isolated fluctuations while preserving edge gradients. The result was the reconstruction shown in Fig. 6. Note that the edge artifacts are now gone, while the edge gradients remain high; in fact, these are improved over those in Fig. 5. Also, the interior of the airplane is now more uniformly bright, as in the ground truth Fig. 2. Finally, the geometry of the airplane is not distorted. However, there is one drawback to this operation. A median cannot distinguish between one-point noise fluctuations and one-point signal fluctuations. Hence, all isolated or semi-isolated point sources are removed, even true ones such as the isolated point source to the right, and the wing-, nose- and tail-tips. In the net, however, Fig. 6 seems to be an improvement over Fig. 5.

Data noise case

The commonest type of data noise is probably additive, Gaussian, white noise, due to the dominance of the central limit theorem[19]. For example, this occurs in ISAR data[6,21]. As an acid test of GMEMK, we generated such noise with a standard deviation of 10% of the maximum data modulus value in Fig. 3. The result is the noisy data shown (in log-modulus) in Fig. 7. A comparison of Figs. 3 and 7 shows that the noise is severe: nearly all the signal structure in Fig. 3 is wiped out. Only the central 5x5 frequency values preserve some resemblance to their true values. Also, the outer frame of frequencies (black picture frame) remains blanked out. Hence, we are now attempting bandwidth extrapolation in the presence of significant data noise.

The linear output, i.e., the DFT of the data, is shown in Fig. 8. The airplane details are now nearly obliterated. This conventional output would be of little practical use for identification purposes.

In preparation for GMEMK, we formed bias functions $a_n,\ldots,d_n$ as follows. The data were apodised using a Gaussian taper function of value 16% at the margins, and the DFT was taken. This complex image was then thresholded at intensity values of 50% of the maximum intensity on a given line (row). The resulting complex image was then used as bias functions in the GMEMK algorithm (15). The modulus of the thresholded image is shown in Fig. 9. As mentioned before, its main purpose is to keep the GMEMK output reconstruction at value zero in the airplane background (black) region. But this constraint benefits reconstruction values *within* the airplane as well, since all reconstruction values *together* obey each data constraint. The result will be an improved output, both within the airplane and without.

The GMEMK-median window output is shown in Fig. 10. Comparison with the linear reconstruction of Fig. 8 shows a strong improvement in image fidelity. The background lacks noise, the airplane outline is more faithfully reconstructed, and the structure within the airplane is more uniform.

It is important, also, to compare entropy output Fig. 10 with the linear, bias image of Fig. 9. If output Fig. 10 closely resembled Fig. 9, this would indicate that the entropy algorithm did little over and above the linear, thresholding operation of Fig. 9 to improve the image. For example, if both figures showed the same airplane boundaries this would mean that the subjectively chosen thresholding level was crucial to the quality of the entropy reconstruction. This would be an unsatisfactory result. However, a comparison of Figs. 9 and 10 shows, to the contrary, that the airplane boundaries in the entropy reconstruction are significantly drawn inward from their bias image values, toward the true boundary values (of Fig. 2). Hence, the entropy algorithm works in the intended way.

Although we have displayed intensity images only, it is important to discuss how well the *complex values* of the object were reconstructed. The basic GMEM algorithm attempts to reconstruct both real and imaginary parts, and it does this quite faithfully, at least in application to point-like objects[10]. For the complementary object case of the extended image in Fig. 2, this was also found to be the case. That is, in the GMEMK-median window reconstructions the (real, imaginary) parts of the object were close to (+1, -1) within the airplane boundaries and were close to 0 outside these boundaries. These were the ideal values.

Summary

The basic GMEM algorithm of Bajkova, whose aim is to reconstruct complex objects from a principle of maximum entropy, and which was applied successfully to point like objects[10], has been augmented for a broader range of applications. This is to strongly noisy, severely bandlimited data due to extended objects. The added use of m.a.p. noise rejection, Kullback bias functions, and a three-point median window operation, allows the modified algorithm to successfully reconstruct such objects (see Fig. 8). Also, a modification [Eqs. (24a,b)] of the solution procedure allows row-by-row, and then column-by-column, processing. The advantage gained is to replace one, large two-dimensional problem by a sequence of one-dimensional problems. This strongly reduces core memory requirements during the solution search, and hence potentially allows much larger image fields to be reconstructed.

References

1. D. R. Wehner, *High Resolution Radar* (Artech House, Dedham, Mass., 1987).
2. J. D. Kraus, *Radio Astronomy* (McGraw Hill, New York, 1966).
3. B. R. Frieden, "Restoring with maximum likelihood and maximum entropy," J. Opt. Soc. Am. **62**, 511-518 (1972).
4. P. A. Jansson, *Deconvolution* (Academic, Orlando, 1984).
5. J. P. Burg, "Maximum entropy spectral analysis," paper presented at 37th meting of the Society of Exploration Geophysicists, Oklahoma City (1967); also, Ph.D. thesis, Stanford University, Palo Alto, California, 123 pages.
6. B. Borden, "Maximum entropy regularization in inverse synthetic aperture radar imagery," IEEE Trans. Signal Proc. SP **40**, 969-973.
7. See, e.g., *Maximum-Entropy and Bayesian Methods in Inverse Problems*, eds. C. R. Smith and W. T. Grandy, Jr. (Reidel, Boston, 1985).
8. E. T. Jaynes, "On the rationale of maximum-entropy methods," Proc. IEEE **70**, 939-952 (1982).
9. J. Skilling and S. F. Gull, "Algorithms and Applications," in Ref. 7. Also H. C. Andrews and B. R. Hunt, *Digital Image Restoration* (Prentice-Hall, Englewood Cliffs, New Jersey, 1977).
10. A. T. Bajkova, "The generalization of maximum entropy method for reconstruction of complex functions," Astron. and Astroph. Trans. 1, 313-320 (1992).
11. S. Kullback and R. A. Leibler, "On information and sufficiency," Ann. Math. Statist. **22**, 79-86 (1951).
12. R. S. Hershel, "Numerical restoration of noncoherent object scenes using analytical and statistical constraints," Ph.D. thesis, Univ. of Arizona, 173 pages (1972).

13. E. S. Meinel, "Origins of linear and nonlinear recursive restoration algorithms," J. Opt. Soc. Am. **A3**, 787-799 (1986).

14. J. E. Shore and R. W. Johnson, "Properties of cross-entropy mininization," IEEE Trans. Information Theory **IT-27**, 472-482 (1981).

15. R. Narayan and R. Nityananda, in *Indirect Imaging, Proc. IAU/URSI Symp.*, ed. J. A. Roberts (Cambridge Univ. Press, Cambridge, 1984).

16. B. R. Frieden, "Unified theory for estimating frequency-of-occurrence laws and optical objects," J. Opt. Soc. Am. **73**, 927-938 (1983).

17. H. J. Trussell, "The relationship between image reconstruction by the maximum *a posteriori* method and a maximum entropy method," IEEE Trans. Acoust., Speech, Signal Processing **ASSP-28**, 114-117 (1980).

18. F. B. Hildebrand, *Introduction to Numerical Analysis* (McGraw-Hill, New York, 1956), pp. 447, 451, 453.

19. B. R. Frieden, "A new restoring algorithm for the preferential enhancement of edges," J. Opt. Soc. Am. **66**, 280-283 (1976).

20. B. R. Frieden, *Probability, Statistical Optics and Data Testing, 2nd ed.* (Springer-Verlag, N.Y., 1991), pp. 254-260.

21. D. L. Mensa, *High Resolution Radar Imaging* (Artech House, Dedham, Mass., 1981).

Figure Headings

1. A real function r(t) may be decomposed into positive regions x(t) and negative regions - y(t), with r(t) = x(t) - y(t).

2. Airplane object, 64x64 pixels, with point source to the right. Intensity image is shown. Complex image is (0,0) outside the airplane and (1, -1) inside. Complex point source is (1, -1).

3. The D.F.T. of the complex object in Fig. 2. This is the discrete object spectrum. The logarithm of its modulus is displayed. The outer picture frame of spectral values (shown black) has been removed from the data set. Thus, only fraction 1024/4096 of data space is filled.

4. Linear reconstruction of the data in Fig. 3 by inverse D.F.T. Missing data values in Fig. 3 are padded out by zeros before D.F.T. operation. The modulus image is shown. Blurring and ringing are caused by the missing data.

5. GMEMK output from data in Fig. 3. The modulus is shown. The reference image (not shown) was a smoothed, thresholded version of the image in Fig. 4. The resolution has been increased over that in Fig. 4. The isolated point source is restored, and the edges are crisper, but suffer from overshoot artifacts just within the airplane outline.

6. GMEMK-median window output from data in Fig. 3. The modulus is shown. The reference image was as before. The edges are crisper than in Fig. 5, and the overshoot artifacts are nearly all gone. However, the isolated point source is wiped out as well.

7. Data of Fig. 3 plus 10% additive, Gaussian noise. The data now suffer from strong noise and bandwidth limitations. The picture frame of frequency values remains blanked out. Even within the passband, the higher frequency values (outer ones) are obliterated.

8. Linear reconstruction of the data in Fig. 7 by inverse D.F.T. Missing data values in Fig. 7 are padded out by zeros before the D.F.T. is taken. The airplane image is unacceptably noisy for most purposes.

9. Bias image (modulus shown) to be used in the GMEMK reconstruction. Its main purpose is to provide *a priori* information as to the location of the background region. Even so crude a background estimate strongly aids the reconstruction process.

10. GMEMK-median window output. The modulus is shown. This is significantly improved over the linear output of Fig. 8.

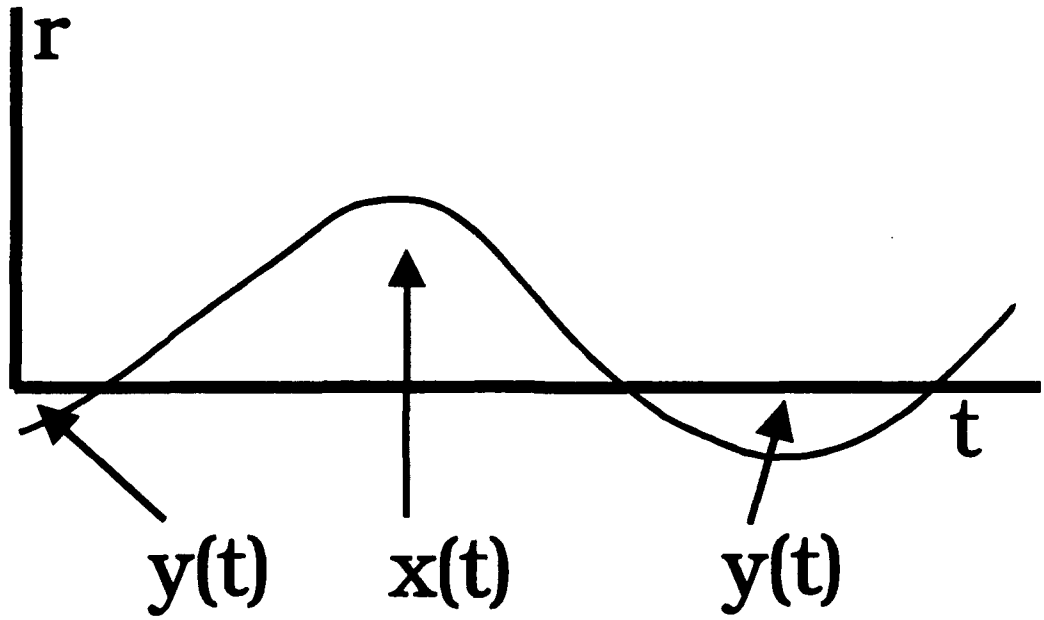

Fig. 1

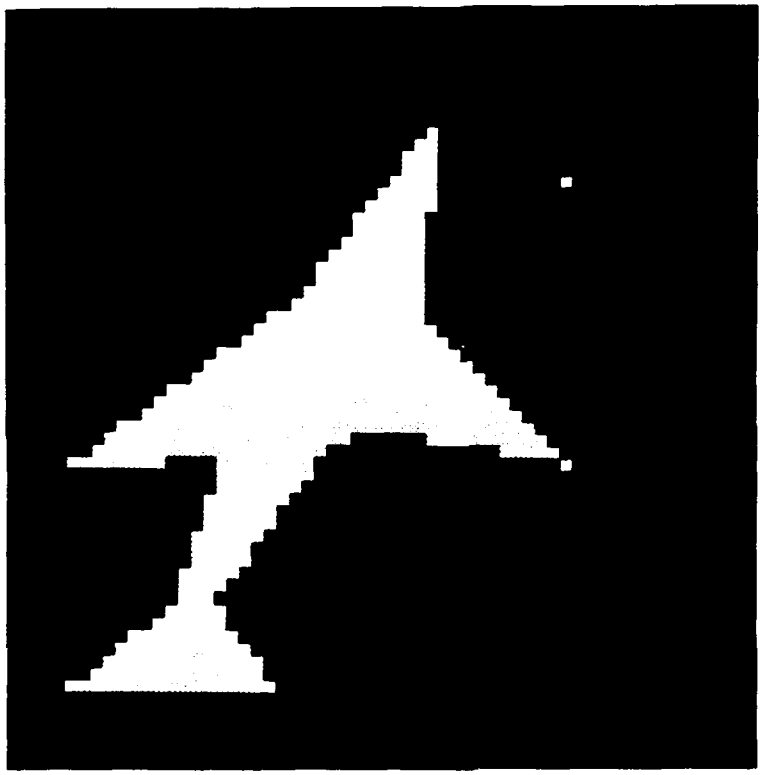

Fig. 2

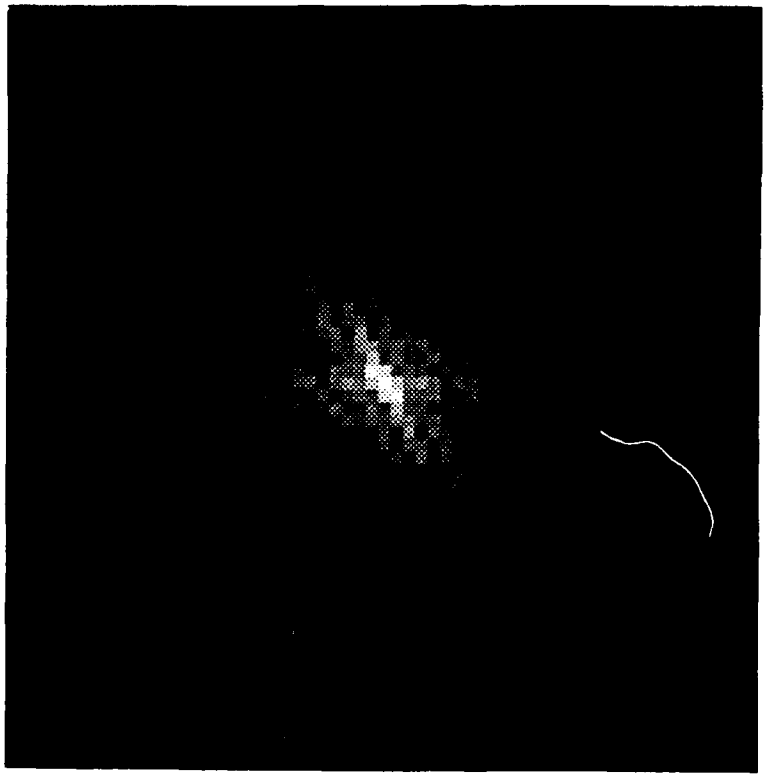

Fig. 3

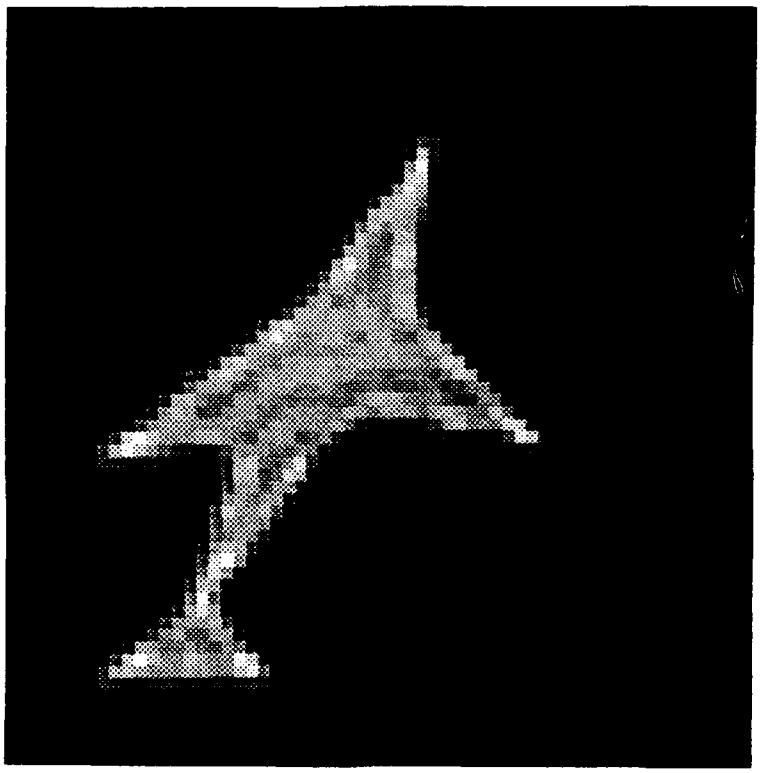

Fig. 4

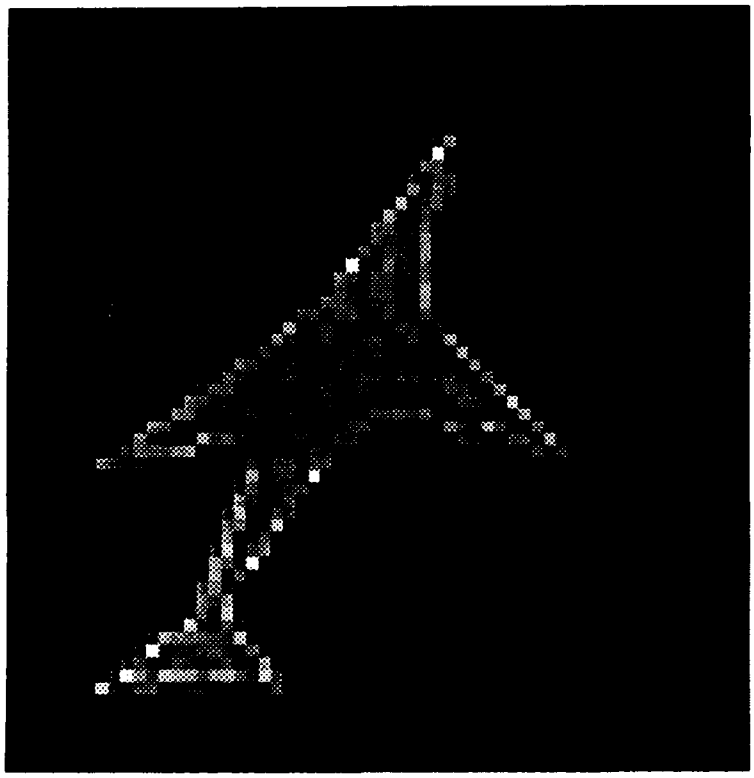

Fig. 5

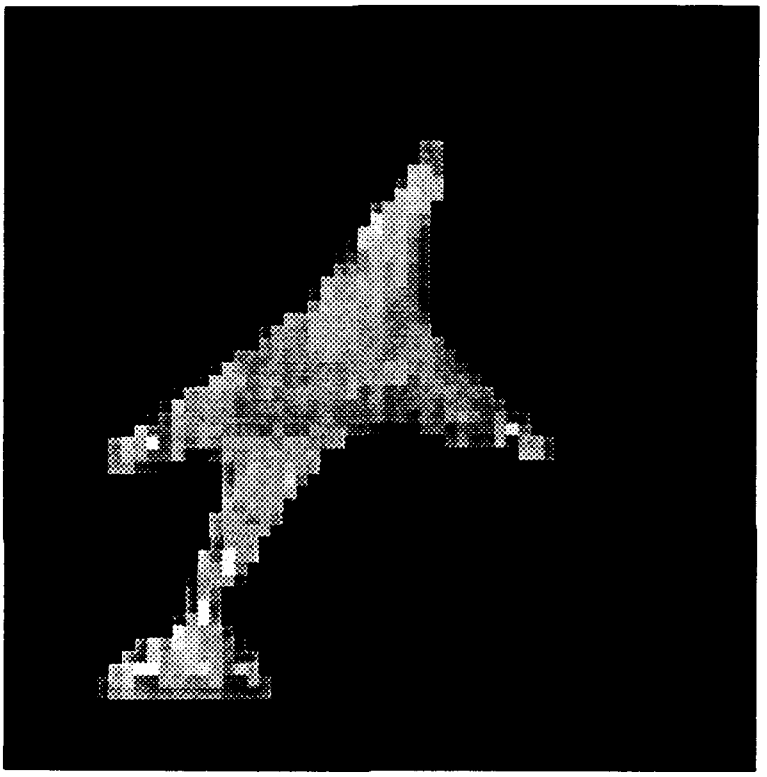

Fig. 6

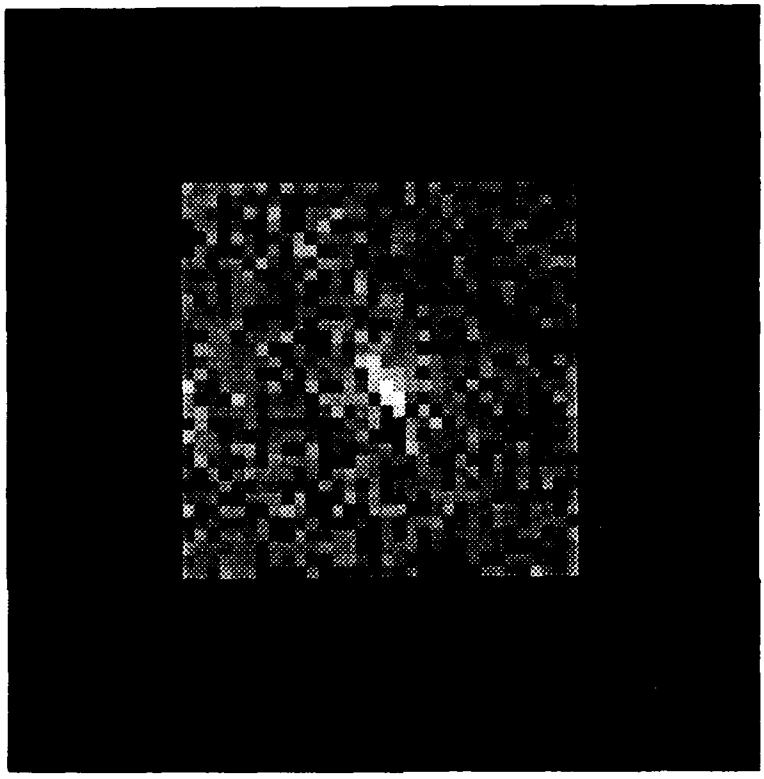

Fig. 7

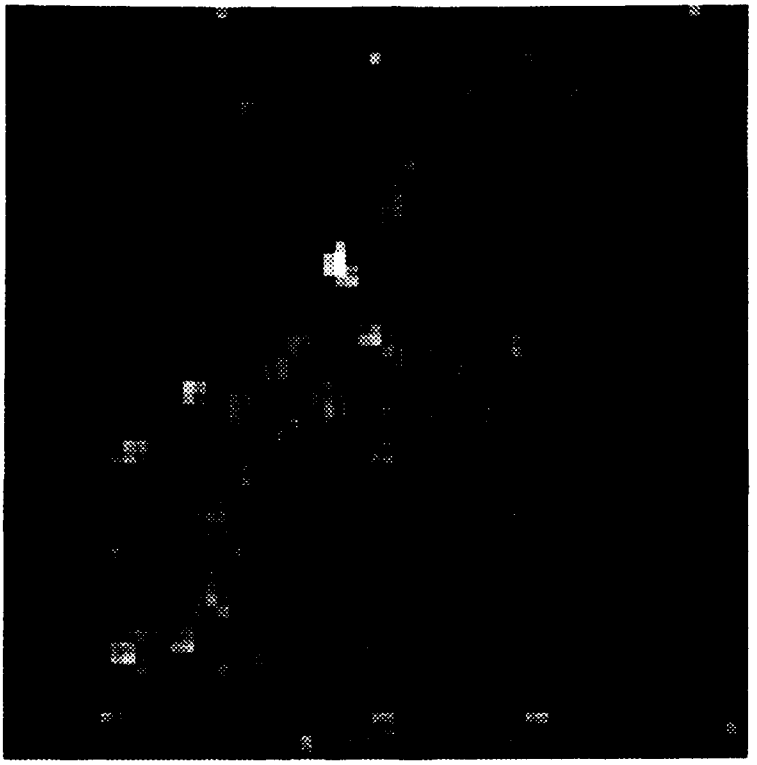

Fig. 8

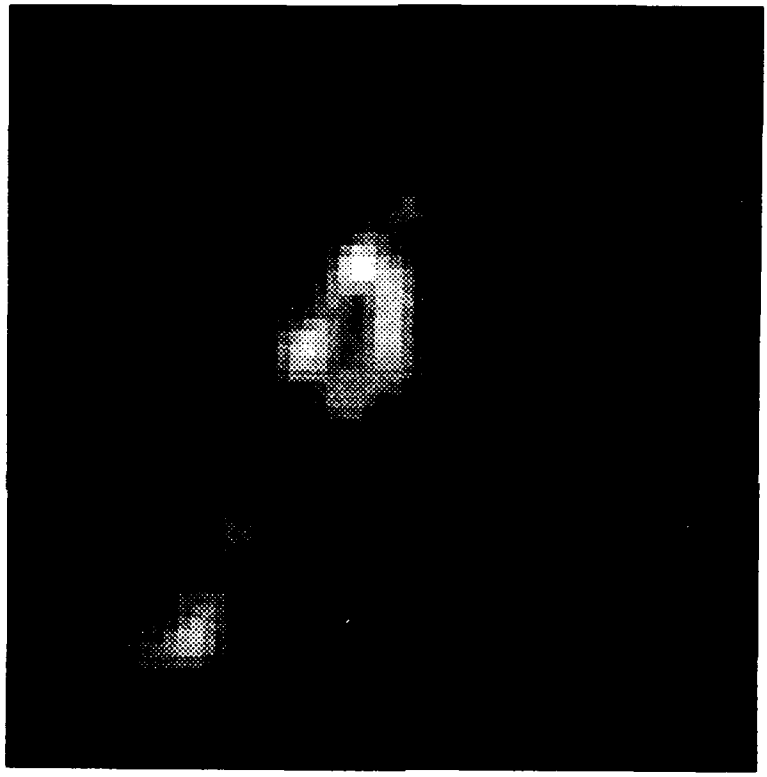

Fig. 9

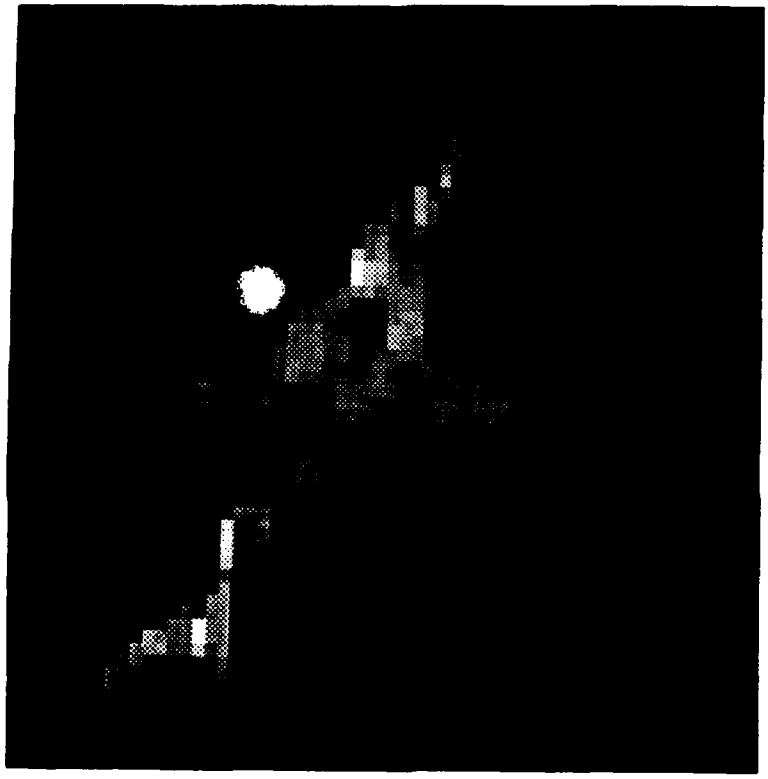

Fig. 10